An improved microgrid arrangement for integrated imaging polarimeters

Daniel A. LeMaster[1,*] and Keigo Hirakawa[2,†]

[1] *Air Force Research Laboratory, 2241 Avionics Circle, Wright-Patterson AFB, OH, USA*

[2] *University of Dayton, 300 College Park, Dayton, OH 45469, USA*

compiled: November 18, 2013

For almost 20 years, microgrid polarimetric imaging systems have been built using a 2×2 repeating pattern of polarization analyzers. In this paper, we show that superior spatial resolution is achieved over this 2×2 case when the analyzers are arranged in a 2×4 repeating pattern. This unconventional result, in which a more distributed sampling pattern results in finer spatial resolution, is also achieved without affecting the conditioning of the polarimetric data reduction matrix. Proof is provided theoretically and through Stokes image reconstruction of synthesized data.

OCIS codes: (110.5405) Polarimetric imaging; (120.5410) Polarimetry

http://dx.doi.org/10.1364/XX.99.099999

1. Introduction

An integrated microgrid imaging polarimeter consists of a repeating pattern of wiregrid polarizers bonded to a focal plane array. The most common microgrid arrangement consists of a 2×2 repeating pattern of analyzer cells [1]. One permutation of the 2×2 array is shown in Figure 1. The lines in each cell correspond to wiregrid element orientation. This pattern was introduced in 1994 [2] and has been standard ever since.

Raw microgrid data are used to infer Stokes parameter images. In 2009, Tyo et al. [3] described how the power spectrum of a raw microgrid image consists of a high bandwidth unmodulated S_0 image spectrum surrounded by the low bandwidth spectra of S_1 and S_2. The S_1 and S_2 spectra are modulated out to the Nyquist frequency in the direction of the principal axes of the array. This is similar to the Color Filter Array (CFA) case where the high bandwidth spectrum centered at DC corresponds to the luminance image and the low bandwidth modulated portions of the spectra correspond to chrominance.

In [4], CFAs are designed to improve spatial resolution by optimizing the separation between the luminance and chrominance spectra. We draw on this approach to propose the new microgrid array pattern shown in Figure 2. This new pattern improves image quality by increasing the spatial bandwidth available for each Stokes image despite the counter-intuitive fact that the new repeating pattern is larger than the original 1994 design. We also show that this new pattern retains the noise performance optimality of the original in terms of conditioning of the data reduction matrix.

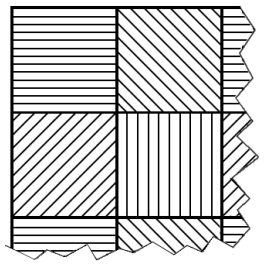

Fig. 1: A conventional 2×2 microgrid array.

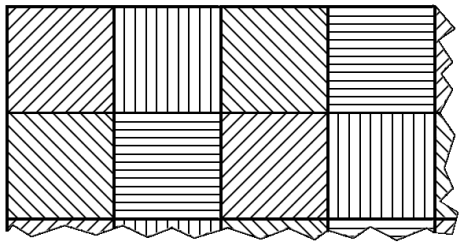

Fig. 2: One permutation of the proposed 2×4 array.

2. Analysis of Microgrid Polarizer Array Sampling

The stokes parameters $= (S_0, S_1, S_2)^T \in \mathbb{R}^3$ follow the standard convention adopted to describe linear polarization states in terms of radiometric quantities. The S_0 image contains grayscale spatial information about the scene. Images S_1 and S_2 together express the extent

* Corresponding author: daniel.lemaster@us.af.mil

† khirakawa1@udayton.edu

and orientation of linear polarization in the scene. The radiation recorded by each detector in a microgrid array $X \in \mathbb{R}^+$ is related to the Stokes parameters S of the incoming light by the equation:

$$X = \underbrace{\begin{bmatrix}\frac{1}{2} & D\cos(2\theta) & D\sin(2\theta)\end{bmatrix}}_{A_\theta} S \tag{1}$$

where, without loss of generality, the neutral density transmission losses in the analyzer are normalized out and $D \in [0,1]$ is the diattenuation of the analyzer is given by

$$D = \frac{p_h^2 - p_v^2}{p_h^2 + p_v^2}. \tag{2}$$

For imaging, the Stokes parameters are a function $S : \mathbb{Z}^2 \to \mathbb{R}^3$, where $S(n)$ is the Stokes parameter for the light arriving at the pixel location $n = (n_1, n_2)^T \in \mathbb{Z}^2$. For imaging with a microgrid polarizer array (MPA), we refer to an array of wiregrid polarizers placed over the entire detector array. As such, the pixel detector at location n makes *exactly one* measurement $X(n)$ ($X : \mathbb{Z}^2 \to \mathbb{R}^+$) along one microgrid polarizer orientation $\theta(n)$ ($\theta : \mathbb{Z}^2 \to \mathbb{R}/2\pi$), as follows:

$$\begin{aligned} X(n) =& A_{\theta(n)} S(n) \\ =& S_0(n) + D\cos(2\theta(n)) S_1(n) \\ &+ D\sin(2\theta(n)) S_2(n) \end{aligned} \tag{3}$$

A finite number of polarizer orientations $\theta \in \{\theta_1, \ldots, \theta_K\}$ are used in MPA. The perspective adopted by the prior work on MPA is that $X(n)$ is a spatial multiplexing of $A_{\theta_k} S(n)$. For instance, the 2×2 repeating MPA pattern takes the following form[3]:

$$\begin{aligned} X(n) &= \begin{cases} A_0(n)S(n) & n_1 \text{ and } n_2 \text{ even} \\ A_{\pi/4}(n)S(n) & n_1 \text{ even; } n_2 \text{ odd} \\ A_{\pi/2}(n)S(n) & n_1 \text{ and } n_2 \text{ odd} \\ A_{3\pi/4}(n)S(n) & n_1 \text{ odd; } n_2 \text{ even} \end{cases} \\ &= S_0(n) + \left(\frac{D}{2}\right)(-1)^{n_1}(S_1(n) + S_2(n)) \\ &\quad + \left(\frac{D}{2}\right)(-1)^{n_2}(S_1(n) - S_2(n)) \end{aligned} \tag{4}$$

Let $\hat{}$ denote discrete space Fourier transform, where $\hat{S}_0(\omega) : \{\mathbb{R}/2\pi\}^2 \to \mathbb{C}$ refers to the Fourier transform of S_0 at the two dimensional spatial frequency $\omega = (\omega_1, \omega_2)^T \in \{\mathbb{R}/2\pi\}^2$, etc. The Fourier analysis of (4) is [3]

$$\begin{aligned} \hat{X}(\omega) =& \hat{S}_0(\omega) + \left(\frac{D}{2}\right)\{\hat{S}_1 + \hat{S}_2\}(\omega - \tbinom{\pi}{0}) \\ &+ \left(\frac{D}{2}\right)\{\hat{S}_1 - \hat{S}_2\}(\omega - \tbinom{0}{\pi}). \end{aligned} \tag{5}$$

This type of Fourier analysis is by now standard in the related field of imaging called color filter array (CFA) [4–6]. By (5), one can reinterpret (4) also as a spatial frequency multiplexing where modulation by $\omega \in \{\binom{\pi}{0}, \binom{0}{\pi}\}$ separates $\hat{S}_1 + \hat{S}_2$ and $\hat{S}_1 - \hat{S}_2$ from $\hat{S}_0$, respectively. The sampling $S \mapsto X$ is said to be *aliased* if the support of $\hat{S}_0(\omega)$ overlaps with $\{\hat{S}_1 + \hat{S}_2\}(\omega - \binom{\pi}{0})$ and/or $\{\hat{S}_1 - \hat{S}_2\}(\omega - \binom{0}{\pi})$. One can use standard amplitude demodulation to reconstruct S_0, S_1, and S_2 from X provided that they are not aliased (see Section 4).

The Fourier support of $\hat{X}$ is shown in the top of Figure 3. Indeed, the modulation of (5) is evidenced by the concentration of energy near $\omega \in \{\binom{0}{0}, \binom{\pi}{0}, \binom{0}{\pi}\}$. This figure is useful for assessing the *risk* of aliasing by the modulation frequency. For instance, if the bandwidth of $\hat{S}_1(\omega)$ is λ (i.e. $\hat{S}_1(\omega) = 0 \ \forall \|\omega\| > \lambda$) then $\hat{S}_0(\omega)$ must be zero $\forall \|\omega\| > \pi - \lambda$ in order to avoid aliasing (a requirement for recovering S from X). It is clear that there is a high risk of aliasing for 2×2 repeating MPA pattern.

3. Proposed: Spatially Optimized MPA

Drawing from the optimal CFA design of [4], consider an alternative to the 2×2 repeating MPA pattern. Suppose $\theta : \mathbb{Z}^2 \to \mathbb{R}/2\pi$ is linear with respect to n:

$$\theta(n) = \frac{1}{2}\omega_0^T n \tag{6}$$

where $\omega_0 \in \mathbb{R}^2$. Letting $Y : \mathbb{Z}^2 \mapsto \mathbb{R}^+$ denote sensor response to this new MPA, $\cos(2\theta(n))$ and $\sin(2\theta(n))$ in Y become sinusoidal modulators:

$$\begin{aligned} Y(n) =& A_{\theta(n)} S(n) \\ =& S_0(n) + D\cos(\omega_0^T n) S_1(n) \\ &+ D\sin(\omega_0^T n) S_2(n). \end{aligned} \tag{7}$$

This gives rise to a straightforward Fourier analysis $\hat{Y}$ of Y:

$$\begin{aligned} \hat{Y}(\omega) =& \hat{S}_0(\omega) + \left(\frac{D}{2}\right)\{\hat{S}_1 - j\hat{S}_2\}(\omega - \omega_0) \\ &+ \left(\frac{D}{2}\right)\{\hat{S}_1 + j\hat{S}_2\}(\omega + \omega_0) \end{aligned} \tag{8}$$

where $j = \sqrt{-1}$. Contrasting (4) and (5) with (7) and (8), respectively, the main difference is that the latter undergoes a spatial frequency modulation by $\omega_0 \in \{\mathbb{R}/2\pi\}^2$. This is evident in the example Fourier support of $\hat{Y}$ shown at the bottom in Figure 3, where $\omega_0 = \binom{\pi/2}{\pi}$ and the energy is concentrated near $\omega \in \{\binom{0}{0}, \binom{\pm\pi/2}{\pi}\}$. Clearly, the advantage of $\hat{Y}$ in (8) over (5) is that the risk of aliasing has reduced significantly because the modulated components of the spectrum are more spread out.

The main conclusion we draw this analysis is that the modulation frequency $\omega_0 \in \{\mathbb{R}/2\pi\}^2$ is a design parameter for MPA patterns which should be chosen to minimize the risk of aliasing. Obviously, choosing $\|\omega_0\|$ to be as large as possible would avoid aliasing between $\hat{S}_0(\omega)$ and $\{\hat{S}_1 - j\hat{S}_2\}(\omega - \omega_0)$. But one must

also consider the risks of aliasing contaminations between $\{\hat{S}_1 - j\hat{S}_2\}(\omega - \omega_0)$ and $\{\hat{S}_1 + j\hat{S}_2\}(\omega + \omega_0)$ which may occur if ω_0 and $-\omega_0$ are close. Hence relative bandwidths of $\hat{S}_0$, $\hat{S}_1$, $\hat{S}_2$ must be simultaneously considered.

4. Image recovery from the optimized MPA

Performance in the presence of noise is unaffected by the new array pattern. For proof, first consider a bandlimited unaliased signal measured with the conventional 2×2 MPA. Demodulation of X yields

$$S_0(n) = H_0(n) \star X(n) \tag{9}$$

$$(D/2)\{S_1(n) + S_2(n)\} = H_1(n) \star \{e^{-j(0,\pi)n} X(n)\} \tag{10}$$

$$(D/2)\{S_1(n) - S_2(n)\} = H_1(n) \star \{e^{-j(\pi,0)n} X(n)\} \tag{11}$$

where $\star$ denotes convolution and H_0 (H_1) are lowpass filters designed to match the support of S_0 (S_1 and S_2). The Fourier domain equivalent of this process is

$$\hat{S}_0(\omega) = \hat{H}_0(\omega)\hat{X}(\omega) \tag{12}$$

$$(D/2)\{\hat{S}_1(\omega) + \hat{S}_2(\omega)\} = \hat{H}_1(\omega)\hat{X}(\omega - \tbinom{0}{\pi}) \tag{13}$$

$$(D/2)\{\hat{S}_1(\omega) - \hat{S}_2(\omega)\} = \hat{H}_1(\omega)\hat{X}(\omega - \tbinom{\pi}{0}) \tag{14}$$

which allows for the Stokes image spectra to be recovered via

$$\begin{pmatrix} \hat{S}_0 \\ \hat{S}_1 \\ \hat{S}_2 \end{pmatrix} = \begin{pmatrix} 1 & 0 & 0 \\ 0 & \frac{1}{D} & \frac{1}{D} \\ 0 & \frac{1}{D} & \frac{-1}{D} \end{pmatrix} \begin{pmatrix} \hat{S}_0 \\ \frac{D}{2}(\hat{S}_1 + \hat{S}_2) \\ \frac{D}{2}(\hat{S}_1 - \hat{S}_2) \end{pmatrix}. \tag{15}$$

Under the same conditions, the 2×4 MPA yields

$$S_0(n) = H_0(n) \star X(n) \tag{16}$$

$$(D/2)\{S_1(n) + jS_2(n)\} = H_1(n) \star \{e^{-j\omega_0^T n} X(n)\} \tag{17}$$

$$(D/2)\{S_1(n) - jS_2(n)\} = H_1(n) \star \{e^{j\omega_0^T n} X(n)\}. \tag{18}$$

and the Stokes spectra are recovered from

$$\begin{pmatrix} \hat{S}_0 \\ \hat{S}_1 \\ \hat{S}_2 \end{pmatrix} = \begin{pmatrix} 1 & 0 & 0 \\ 0 & \frac{1}{D} & \frac{1}{D} \\ 0 & \frac{-j}{D} & \frac{j}{D} \end{pmatrix} \begin{pmatrix} \hat{S}_0 \\ \frac{D}{2}(\hat{S}_1 + j\hat{S}_2) \\ \frac{D}{2}(\hat{S}_1 - j\hat{S}_2) \end{pmatrix}. \tag{19}$$

In both (15) and (19), the matrices that recover the Stokes spectra from the demodulation products have the same condition number, e.g. for $D = 1$ the condition number of each is $\frac{1}{\sqrt{2}}$. Both MPA are equally conditioned and therefore expected to provide equivalent performance in the presence of noise.

5. Demonstration using synthetic imagery

Synthetic imagery is used in this section to demonstrate the wider unaliased bandwidth and thus superior image quality of the 2×4 array. Raw microgrid data of each array type are generated from Stokes imagery of a static scene originally collected with a visible Rotating Analyzer (RA) imaging polarimeter. Before microgrid resampling, the total bandwidth of each RA Stokes images was limited using an 11×11 pixel Gaussian filter with a 0.5 pixel standard deviation. The log-scale spectra in Figure 3 show that the 2×4 array reduces the risk of aliasing by further separating out the various polarimetric image components. The conversion from Stokes to raw microgrid data is accomplished via (7). The modeled microgrid analyzers have unity diattenuation. Both sets of microgrid data are demosaicked using the method described in Section 4. For both the 2×2 and 2×4 cases, all Gaussian reconstruction filters has a support of 41×41 pixels and standard deviation of 1 pixel.

More importantly, this difference in array arrangement is manifest in the reconstructed S_0 and Degree of Linear Polarization (DOLP) images. DOLP, $P(n)$ ($P : \mathbb{Z}^2 \to \mathbb{R}^+/1$) is recoverable from the Stokes images by the relation:

$$P(n) = \frac{\sqrt{S_1^2(n) + S_2^2(n)}}{S_0(n)}. \tag{20}$$

Physically, DOLP is a measure of the extent of polarization inferred for each pixel in the scene. Aliasing in microgrid imagery is readily observable as false DOLP signals.

The reconstructed S_0 and DOLP images for each array configuration are shown in Figures 4 and 5. The 2×2 array results are clearly more aliased than their 2×4 counterparts but the difference is especially noticeable throughout the DOLP images.

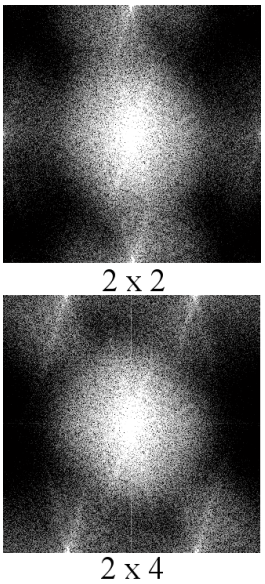

Fig. 3: The log-scale spectra of MPA sampled sensor data.

6. Summary and discussion

We believe that the polarimetric sampling arrangement introduced in this paper represents the first major improvement in spatial resolution for microgrid integrated imaging polarimeters in almost 20 years. This improved array widens the unaliased bandwidth available for image reconstruction by increasing the separation between

2 x 2

2 x 4

Fig. 4: Reconstructed S_0 images.

2 x 2

2 x 4

Fig. 5: Reconstructed DOLP images.

the spatially modulated Stokes components of the microgrid spectra. This outcome is achieved without affecting performance in the presence of noise. The veracity of these claims is developed theoretically and demonstrated using realistic synthetic imagery.

This work would be incomplete without several final points. First, the relationship between components of the microgrid spectra are a consequence of the periodic sampling array and independent of detector size. Consequently, this refined microgrid pattern will be useful even as the technology to produce smaller detectors and microgrids continues to improve. Second, it should be obvious that the 2×4 pattern presented here has multiple equally valid permutations and their transposes.

References

[1] J. S. Tyo, D. L. Goldstein, D. B. Chenault, and J. A. Shaw, Appl. Opt. **45**, 5453 (2006).

[2] C. S. L. Chun, D. L. Fleming, and E. J. Torok, Proc. SPIE **2234**, 275 (1994).

[3] J. S. Tyo, C. F. LaCasse, and B. M. Ratliff, Opt. Lett. **34**, 3187 (2009).

[4] K. Hirakawa and P. J. Wolfe, Image Processing, IEEE Transactions on **17**, 1876 (2008).

[5] D. Alleysson, S. Susstrunk, and J. Hérault, Image Processing, IEEE Transactions on **14**, 439 (2005).

[6] B. Leung, G. Jeon, and E. Dubois, Image Processing, IEEE Transactions on **20**, 1885 (2011).

Full References

In this section, please provide full versions of citations to assist reviewers and editors (OL publishes a short form of citations) or any other information that would aid the peer-review process.

References

[1] J. S. Tyo, D. L. Goldstein, D. B. Chenault, and J. A. Shaw, "Review of passive imaging polarimetry for remote sensing applications," Appl. Opt. **45**, 5453–5469 (2006).

[2] C. S. L. Chun, D. L. Fleming, and E. J. Torok, "Polarization-sensitive thermal imaging," Proc. SPIE **2234**, 275–286 (1994).

[3] J. S. Tyo, C. F. LaCasse, and B. M. Ratliff, "Total elimination of sampling errors in polarization imagery obtained with integrated microgrid polarimeters," Opt. Lett. **34**, 3187–3189 (2009).

[4] K. Hirakawa and P. J. Wolfe, "Spatio-spectral color filter array design for optimal image recovery," Image Processing, IEEE Transactions on **17**, 1876–1890 (2008).

[5] D. Alleysson, S. Susstrunk, and J. Hérault, "Linear demosaicing inspired by the human visual system," Image Processing, IEEE Transactions on **14**, 439–449 (2005).

[6] B. Leung, G. Jeon, and E. Dubois, "Least-squares luma–chroma demultiplexing algorithm for bayer demosaicking," Image Processing, IEEE Transactions on **20**, 1885–1894 (2011).